

# 000 001 002 003 004 005 DYNAMICALLY GATED MIXTURE OF EXPERTS FOR 006 MULTI-TASK REINFORCEMENT LEARNING 007 008 009

010 **Anonymous authors**  
011 Paper under double-blind review  
012  
013  
014  
015  
016  
017  
018  
019  
020  
021  
022

## 023 ABSTRACT 024

025 Multi-task reinforcement learning (MTRL) promises unique strengths against  
026 single-task RL because of generalization across tasks through parameter sharing  
027 and composition. Existing methods rely on local routing or static compositional  
028 weights in Mixture-of-Experts (MoE) without the ability to adapt to evolving tem-  
029 poral context. To improve the inherently temporal and dynamic systems in MTRL,  
030 we introduce a global recurrent inhibition network (GRIN) that performs dynamic  
031 gating across time, selectively modulating expert activations based on temporally  
032 accumulated context. Our formulation propagates information across time steps  
033 to preserve global activation information across the model. Notably, using the gat-  
034 ing approach, we found statistically significant improvements over state-of-the-art  
035 MTRL methods, with an empirical **+3.7%** improvement on the Metaworld MT50  
036 benchmark.  
037  
038

## 039 1 INTRODUCTION 040

041 Deep reinforcement learning has demonstrated the capacity to acquire complex behaviors across  
042 diverse domains Mnih et al. (2013); Gu et al. (2017); Kalashnikov et al. (2018); Lillicrap et al.  
043 (2015). The human ability to leverage similar tasks to learn to perform many tasks inspires multi-  
044 task reinforcement learning (MTRL), which offers a path toward more general agents. To enable  
045 sharing of knowledge and parameters, Mixture-of-experts and compositional parameter-sharing ap-  
046 proaches Hendawy et al. (2023); Sun et al. (2022) have shown promise by enabling task-specific  
047 specialization within unified architectures. However, these methods typically rely on local routing  
048 or static compositional weights, limiting adaptability as temporal context evolves during an episode.  
049

050 Gating mechanisms have proven effective for controlling information flow in neural networks, such  
051 as LSTMs Hochreiter & Schmidhuber (1997) and notably, to modern attention and LLM architec-  
052 tures Qiu et al. (2025). Recent work Qiu et al. (2025) demonstrates that dynamic, input-dependent  
053 gating applied across time enhances nonlinear expressivity and improves optimization stability. We  
054 investigate whether these benefits extend to the complex temporal dynamics of MTRL, where agents  
055 must continuously adapt behavior based on evolving task demands. We introduce a global recurrent  
056 inhibition network (GRIN) that performs dynamic gating across time steps, selectively modulating  
057 feature activations based on temporally accumulated context.  
058

059 A key challenge in applying gating to model-free deep RL is that feedforward networks restrict  
060 gating inputs to preceding layers within the current forward pass, forfeiting access to global in-  
061 formation. Our formulation addresses this by propagating activations forward across time steps,  
062 enabling the gate to leverage any activation from the previous step and preserve global context.  
063 This mechanism directly parallels cortical inhibitory neurons that integrate diverse synaptic inputs  
064 to orchestrate neural computation.  
065

066 We show that in multi-task settings, global network gating with input access to Q-value and task-  
067 specific signals enhances model performance. GIN achieves 90.0% on the Metaworld MT10 bench-  
068 mark, and demonstrates a statistically significant **+3.7%** improvements with our reproduced results  
069 on the challenging MT50 benchmark. These results demonstrate that temporal gating yields im-  
070 provements over state-of-the-art MTRL methods, establishing dynamic gating across time as an  
071 effective mechanism for multi-task policy learning.  
072

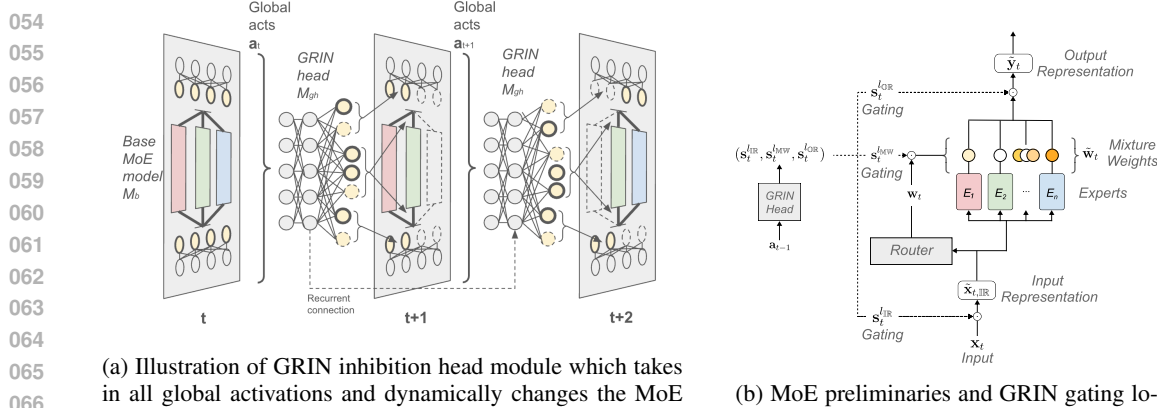


Figure 1: Model Architecture

## 2 BACKGROUND AND RELATED WORK

A rich body of work in MTRL has explored diverse strategies for achieving effective generalization across tasks. The paper D’Eramo et al. (2024) established theoretical foundations showing that MTRL yields increasing benefits as the number of tasks grows, while Teh et al. (2017) propose learning individual task policies that share a common prior. The Meta-World benchmark Yu et al. (2020b) has become a standard testbed for robotic manipulation, typically trained with Soft Actor-Critic Haarnoja et al. (2018). However, naive parameter sharing can induce negative transfer when task gradients conflict. The paper Yu et al. (2020a) address this through gradient projection methods that orthogonalize task gradients, though such approaches can be sensitive to gradient variance. Modular architectures offer an alternative: Yang et al. (2020) introduce routing networks that generate task-specific parameters from a shared base model, and Devin et al. (2017) decompose policy responsibilities across robot-specific and task-specific modules. More recent work conditions shared representations on task context: Sodhani et al. (2021) learn a mixture of state encoders using task metadata, producing diverse and interpretable representations, while Perez et al. (2018) leverages feature-wise linear modulation for task conditioning.

Deep learning has designed adaptation and inhibitive mechanisms through learnable gating architectures that selectively amplify or suppress features. These appear in LSTMs (Hochreiter & Schmidhuber, 1997), Highway Networks (Srivastava et al., 2015), and Gated Linear Units (GLUs) (Dauphin et al., 2017b; Shazeer, 2020), where they prevent gradient vanishing, and enhance network sparsity. The mechanism mirrors biological cortical inhibition, where diverse inhibitory neurons modulate excitatory activity to maintain network stability and sharpen signal selectivity (Isaacson & Scanziani, 2011; Klausberger & Somogyi, 2008; Tremblay et al., 2016). Studies reveal remarkable diversity in inhibitory connectivity patterns inhibition (Gidon & Segev, 2012; Markram et al., 2004; Chini et al., 2022).

Dropout and its variants (Ba & Frey, 2013; Kingma et al., 2015; Ghiasi et al., 2018; Liu et al., 2022; Zhao et al., 2022; Li et al., 2023) demonstrate the effectiveness of stochastic adaptation during training. Capsules (Hinton et al., 2011; Sabour et al., 2017; Hinton et al., 2018) leverage dynamic routing at the unit and layer level, and remains an area of novel active research. In comparison, we focus on a global approach to improve existing ML models and MoE.

Different from prior work, we propose a global approach across the model. The propagation across time builds a global, dynamic adaptation module. This module aggregates signals from any part of the neural network and modulate MoE pathways. This design enables GRIN to provide a general mechanism for dynamic modulation. We demonstrate its effectiveness in multi-task reinforcement learning, as well as in computer vision and limited-scale language models.

108 

### 3 ALGORITHM AND METHODS

109 

#### 3.1 PRELIMINARIES

110 Mixture of Experts (MoE) (Shazeer et al., 2017) architectures dynamically route inputs through  
 111 specialized sub-networks. A standard MoE layer transforms an input representation (IIR)  $\mathbf{x}_{\text{IIR}} \in$   
 112  $\mathbb{R}^d$ . In an MoE without a router model (Sun et al., 2022),  $\mathbf{x}_{\text{IIR}}$  is transformed by the experts then  
 113 aggregated by mixture weights (MW) which could be either fixed or learned. In a gated MoE,  
 114  $\mathbf{x}_{\text{IIR}}$  is put to a router model that computes mixture weights  $\mathbf{w}_{\text{MW}} = \text{Router}(\mathbf{x}_{\text{IIR}})$ , and  $\mathbf{w}_{\text{MW}} =$   
 115  $[w_1, w_2, \dots]$  where  $w_i$  represents the contribution of the  $i$ -th expert out of  $N$  experts. After  $\mathbf{x}_{\text{IIR}}$   
 116 is propagated through the expert models, an aggregation step combines expert outputs. The final  
 117 output representation (OR) is computed as:  $\mathbf{y}_{\text{OR}} = \sum_{i=1}^N w_i \cdot E_i(\mathbf{x}_{\text{IIR}})$ , where  $E_i$  denotes the  
 118  $i$ -th expert network and  $N$  is the total number of experts. Variants include mixed MoE where all  
 119 experts process inputs with soft weights from a softmax router, gated MoE that adds learnable gates  
 120 to modulate expert contributions, and sparsely-gated MoE that selects only the top- $k$  experts for  
 121 efficiency.

122 To enable precise control over network modulation, we design the GRIN head module to dynamically  
 123 regulate MoE architectures. Generic MoE leverages three key representations: the input rep-  
 124 resentation (IIR), the mixture weights (MW), and the output representation (OR). The GRIN head  
 125 module generates gating masks through sigmoid non-linearity (Dauphin et al., 2017a), directly mod-  
 126 ulating these representations.

131 

#### 3.2 GRIN ARCHITECTURE WITH THE HEAD MODULE

132 The limitation of existing MoE approaches is that gating decisions are made locally based solely  
 133 on the current input representation  $\mathbf{x}_{\text{IIR}}$ , without considering global network activation patterns or  
 134 interactions between experts. We propose Global Recurrent Inhibition Networks (GRIN) that mod-  
 135 ulate the MoE architecture at three critical locations<sup>1</sup>—input representations (IIR), mixture weights  
 136 (MW), and output representations (OR)—using inhibition masks ( $\mathbf{s}$ ) derived from global network  
 137 activations:

$$140 \quad \tilde{\mathbf{a}}^l = \mathbf{s}^l \odot \mathbf{a}^l, \quad \text{for } l \in \{l_{\text{IIR}}, l_{\text{MW}}, l_{\text{OR}}\} \quad \text{where } \mathbf{s}^{l_{\text{IIR}}}, \mathbf{s}^{l_{\text{MW}}}, \mathbf{s}^{l_{\text{OR}}} = \sigma(\mathcal{G}(\mathbf{a}_{\text{global}})). \quad (1)$$

141 Here  $\mathbf{a}^l$  denotes the original activation at location  $l$ ,  $\mathbf{s}^l$  denotes the inhibition mask computed by the  
 142 GRIN head  $\mathcal{G}$  from global activations  $\mathbf{a}_{\text{global}}$  with the ending sigmoid non-linearity  $\sigma$ ,  $\odot$  denotes  
 143 element-wise multiplication, and  $\tilde{\mathbf{a}}^l$  denotes the gated activation. This formulation enables dynamic,  
 144 globally-aware modulation that considers the full network state when making modulation and gating  
 145 decisions.

146 As shown in Figure 1a and Figure 1b, the GRIN head model operates as a modulator and controller,  
 147 taking in the global activations and producing the inhibition masks. The inhibition masks are applied  
 148 to elements of the MoE model, on mixture weights ( $l_{\text{MW}}$ ) of the MoE model, which determines  
 149 the weighting or selection of each expert. The other category of gating for the GRIN head is to  
 150 modulate and modify the input representation ( $l_{\text{IIR}}$ ) as well as the output representation ( $l_{\text{OR}}$ ) of the  
 151 MoE model.

152 For a base model with MoE architecture, GRIN is defined as  $\Gamma = (\mathcal{X}, \mathcal{M}, \mathcal{G}, \mathcal{A}, \mathcal{S}, \mathcal{L})$ , where  $\mathcal{X}$   
 153 denotes input data,  $\mathcal{M}$  is the base MoE model,  $\mathcal{G}$  is the GRIN head,  $\mathcal{A}$  represents base model  
 154 activations,  $\mathcal{S}$  are the inhibition masks (gating masks), and  $\mathcal{L}$  specifies gating target locations, and  
 155  $\mathcal{L} = \{l_{\text{IIR}}, l_{\text{MW}}, l_{\text{OR}}\}$ . The system evolves through discrete time steps with state representations  
 156  $\mathcal{D} = \{(\mathbf{x}_t, \mathbf{a}_t, \mathbf{h}_t, \mathbf{s}_t)\}$ , where  $\mathbf{x}_t \in \mathbb{R}^n$ ,  $\mathbf{a}_t \in \mathbb{R}^m$ ,  $\mathbf{h}_t \in \mathbb{R}^k$ , and  $\mathbf{s}_t \in \mathbb{R}^p$ .

157 <sup>1</sup>We define a location to be one or more layers, units or connections in the network.

**Algorithm 1** GRIN Forward Pass

---

```

162
163 Require: Input  $\mathbf{x}_t$ , Number of recurrent steps  $T$ , GRIN head  $\mathcal{G}$ , base model
164    $\mathcal{M}$ 
165   1: for  $iter = 1$  to  $N$  do
166     2: Initialize  $\mathbf{s}_0 \leftarrow 1$ ,  $\mathbf{h}_0, \mathbf{h}_{-1}$ 
167     3: for  $t = 1$  to  $T$  do
168       4:  $\mathbf{h}_{t-1} \leftarrow f_{\text{RNN}}(\mathbf{h}_{t-2}, \tilde{\mathbf{a}}_{t-1})$   $\triangleright$  Update hidden state
169       5:  $\mathbf{s}_t^{l_{\text{IR}}}, \mathbf{s}_t^{l_{\text{MW}}}, \mathbf{s}_t^{l_{\text{OR}}} \leftarrow \sigma(\mathbf{W}_{\text{GRIN}} \mathbf{h}_{t-1} + \mathbf{b}) = \sigma(\mathcal{G}(\mathbf{h}_{t-2}, \tilde{\mathbf{a}}_{t-1}))$ 
170       6:  $\mathbf{a}_t^{l_{\text{IR}}}, \mathbf{a}_t^{l_{\text{pretext}}} \leftarrow \mathcal{M}_{\text{Pretext}}(\mathbf{x}_t)$   $\triangleright$  Forward pretext model
171       7:  $\tilde{\mathbf{a}}_t^{l_{\text{IR}}} \leftarrow \mathbf{s}_t^{l_{\text{IR}}} \odot \mathbf{a}_t^{l_{\text{IR}}}$   $\triangleright$  Modulate input repres.
172       8:  $\mathbf{w}_t \leftarrow \text{Router}(\tilde{\mathbf{a}}_t^{l_{\text{IR}}})$   $\triangleright$  Compute mixture weights
173       9:  $\tilde{\mathbf{w}}_t \leftarrow \mathbf{s}_t^{l_{\text{MW}}} \odot \mathbf{w}_t$   $\triangleright$  Modulate mixture weights
174      10:  $\mathbf{a}_t^{l_{\text{OR}}} \leftarrow \sum_{i=1}^N \tilde{w}_{i,t} \cdot E_i(\tilde{\mathbf{a}}_t^{l_{\text{IR}}})$   $\triangleright$  Aggregate outputs
175      11:  $\tilde{\mathbf{a}}_t^{l_{\text{OR}}} \leftarrow \mathbf{s}_t^{l_{\text{OR}}} \odot \mathbf{a}_t^{l_{\text{OR}}}$   $\triangleright$  Modulate output
176      12:  $\mathbf{a}_t^{\text{post}} \leftarrow \mathcal{M}_{\text{post}}(\tilde{\mathbf{a}}_t^{l_{\text{OR}}})$   $\triangleright$  Forward post model
177      13:  $\tilde{\mathbf{a}}_t \leftarrow \{\mathbf{a}_t^{\text{pretext}}, \tilde{\mathbf{a}}_t^{l_{\text{IR}}}, \tilde{\mathbf{a}}_t^{l_{\text{OR}}}, \mathbf{a}_t^{\text{post}}\}$   $\triangleright$  Aggregate activations
178      14: Compute losst
179      15: BackProp losst
180      16:  $\theta \leftarrow \theta + \Delta\theta$ 
181      17: end for
182      18: end for

```

---

**3.3 GRIN RECURRENT FORMULATION**

GRIN employs a recurrent formulation where the inhibition masks are iteratively refined over  $T$  time steps, allowing the network to observe and respond to its own activation patterns. As shown in Figure 2, at each timestep  $t$ , the GRIN head processes the current gated activations  $\tilde{\mathbf{a}}_t$ , the hidden state  $\mathbf{h}_t$ , and the previous hidden state  $\mathbf{h}_{t-1}$  to compute updated inhibition masks  $\mathbf{s}_{t+1}$ , which modulate the network’s forward pass. This recurrent mechanism enables the network to iteratively refine the modulation of expert weights and representations by incorporating feedback from previous choices. The state evolution is governed by the following dynamics:

$$\begin{aligned}
191 \quad \mathbf{h}_t &= f_{\text{RNN}}(\mathbf{h}_{t-1}, \tilde{\mathbf{a}}_t) \\
192 \quad \mathbf{s}_{t+1} &= \sigma(\mathbf{W}_{\text{GRIN}} \cdot \mathbf{h}_t + \mathbf{b}) = \sigma(\mathcal{G}(\mathbf{h}_{t-1}, \tilde{\mathbf{a}}_t)) \\
193 \quad \tilde{\mathbf{a}}_{t+1}^{l_{\text{OR}}} &= \mathcal{M}_{\text{MoE}}(\mathbf{x}_{\text{IR}} \odot \mathbf{s}_t^{l_{\text{IR}}}, \mathbf{w}_{\text{MW}} \odot \mathbf{s}_t^{l_{\text{MW}}}) \odot \mathbf{s}_t^{l_{\text{OR}}}
\end{aligned} \tag{2}$$

where  $f_{\text{RNN}}$  can be any recurrent cell (LSTM, GRU),  $\mathbf{s}_t = \{\mathbf{s}_t^{l_{\text{IR}}}, \mathbf{s}_t^{l_{\text{MW}}}, \mathbf{s}_t^{l_{\text{OR}}}\}$  are the inhibition masks at timestep  $t$ , and  $\mathcal{M}_{\text{MoE}}(\cdot)$  denotes the modulated MoE forward pass using inhibition masks  $\mathbf{s}_t$ . During training, gradients flow through all timesteps via backpropagation through time, jointly optimizing the base model and GRIN head. Algorithm 1 presents the full GRIN recurrent algorithm.

**3.4 TRAINING, OPTIMIZATION, AND INFERENCE**

During training and across recurrence steps, the gradient computation graph is kept and we perform gradient back-propagation across time to optimize the recurrent neural network. We note that in the case of GRIN, when the data input is non-sequential, we choose to use the same  $\mathbf{x}$  to propagate multiple time-steps. This simulates the dynamic changes in the base-model with the same data input, but across different time steps. When we use GRIN to recurrently forward propagate  $T$  steps, it is a choice to back-propagate at each time step, and sum the gradients over time. This offers a higher quality gradient for the optimization. At inference time, the pretext inhibition and GRIN models can operate on the data points sampled from the test set.

**4 EXPERIMENTS ON MULTI-TASK REINFORCEMENT LEARNING**

We evaluate the GRIN algorithm on the MetaWorld benchmark with the multi-task reinforcement learning (MTRL). MetaWorld offers a suite of reinforcement learning environments comprising up to 50 robotic manipulation tasks. In our RL model, both the actor and critic networks employ Mixture-of-Experts (MoE) architectures with orthogonalization, while the mixture-weight encoder is conditioned solely on the task-ID.

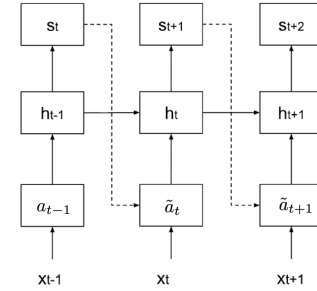


Figure 2: Recurrent network for GRIN with respect to activations, hidden states, and inhibition masks.

216  
217 Table 1: MT10 Average Success Rate (%): comparison of GRIN with prior methods  
218

Method	Epoch 1 % (1M)	Epoch 2 % (2M)	Epoch 3 % (3M)	Epoch 5 % (5M)	Epoch 10 % (10M)	Epoch 15 % (15M)	Epoch 20 % (20M)
SAC (Yu et al., 2019)	10.0 $\pm$ 8.2	17.7 $\pm$ 2.1	18.7 $\pm$ 1.1	20.0 $\pm$ 2.0	48.0 $\pm$ 9.5	57.7 $\pm$ 3.1	61.9 $\pm$ 3.3
MTSAC (Yu et al., 2019)	34.9 $\pm$ 12.9	49.3 $\pm$ 9.0	57.1 $\pm$ 9.8	60.2 $\pm$ 9.6	61.6 $\pm$ 6.7	65.6 $\pm$ 10.4	62.9 $\pm$ 8.0
SAC+FiLM (Perez et al., 2017)	32.7 $\pm$ 6.5	46.9 $\pm$ 9.4	52.9 $\pm$ 6.4	57.2 $\pm$ 4.2	59.7 $\pm$ 4.6	61.7 $\pm$ 5.4	58.3 $\pm$ 4.3
PCGrad (Yu et al., 2020)	32.2 $\pm$ 6.8	46.6 $\pm$ 9.3	54.0 $\pm$ 8.4	60.2 $\pm$ 9.7	62.6 $\pm$ 11.0	62.6 $\pm$ 10.5	61.7 $\pm$ 10.9
Soft-Module (Yang et al., 2020)	24.2 $\pm$ 4.8	41.0 $\pm$ 2.9	47.4 $\pm$ 5.3	51.4 $\pm$ 6.8	53.6 $\pm$ 4.9	56.6 $\pm$ 4.8	63.0 $\pm$ 4.2
CARE (Sodhani et al., 2021)	26.0 $\pm$ 9.1	52.6 $\pm$ 9.3	63.8 $\pm$ 7.9	66.5 $\pm$ 8.3	69.8 $\pm$ 5.1	72.2 $\pm$ 7.1	76.0 $\pm$ 6.9
PaCo (Sun et al., 2022)	30.5 $\pm$ 9.5	49.8 $\pm$ 8.2	65.7 $\pm$ 4.5	64.7 $\pm$ 4.2	71.0 $\pm$ 5.5	81.0 $\pm$ 5.9	85.4 $\pm$ 4.5
MOORE (Hendawy et al., 2024)	36.4 $\pm$ 7.8	64.4 $\pm$ 5.5	72.1 $\pm$ 6.5	74.8 $\pm$ 4.0	80.1 $\pm$ 6.1	84.8 $\pm$ 4.3	88.4 $\pm$ 3.4
<b>MOORE (IQM<math>\pm</math>std)</b>	<b>33.5<math>\pm</math>4.3</b>	<b>65.0<math>\pm</math>4.0</b>	<b>72.8<math>\pm</math>4.0</b>	<b>74.2<math>\pm</math>3.3</b>	<b>79.8<math>\pm</math>0.4</b>	<b>84.8<math>\pm</math>4.3</b>	<b>89.5<math>\pm</math>0.3</b>
GRIN (Ours)	<b>45.7<math>\pm</math>9.1</b>	63.7 $\pm$ 3.0	68.3 $\pm$ 5.3	<b>78.4<math>\pm</math>5.8</b>	<b>83.0<math>\pm</math>4.4</b>	<b>87.7<math>\pm</math>3.5</b>	<b>89.4<math>\pm</math>1.0</b>
GRIN (Ours, IQM $\pm$ std)	<b>45.4<math>\pm</math>5.0</b>	<b>63.3<math>\pm</math>0.4</b>	<b>69.0<math>\pm</math>1.7</b>	<b>78.3<math>\pm</math>0.4</b>	<b>81.5<math>\pm</math>2.6</b>	<b>89.4<math>\pm</math>0.9</b>	<b>90.0<math>\pm</math>0.0<sup>4</sup></b>

229  
230 Aligned with the experiment procedures of the previous work, we use the soft-actor-critic (SAC)  
231 model with a 3-layer fully connected neural network each with 400 hidden units and  $tanh$  non-  
232 linearity. We use 4 experts MoE model for the MT10 experiment and 6 experts MoE for the MT50  
233 experiment. The multi-head architecture is used after the MoE. Our experiments are performed with  
234 GRIN gating on both  $l_{\text{MW}}$ , and  $l_{\text{OR}}$  locations, and implemented in the MoE algorithm with task-  
235 encoder (Sun et al., 2022) and orthogonalization (Hendawy et al., 2023). The MoE architecture and  
236 GRIN are used for both Actor and Critic networks, but GRIN does not have connections across the  
237 two network. In each epoch we run the soft-actor-critic algorithm with GRIN for 100,000 iterations,  
238 with batch size of 128. **For evaluation, we follow Agarwal et al. (2021) to compute the interquartile**  
239 **mean (IQM) of success rates across random seeds for both MT10 and MT50.** Robust to outlier  
240 scores, the IQM computes the mean on the middle 50% of combined runs, after ranking the random  
241 seeds with their success rates. For the standard deviation calculation in the IQM column of the  
242 tables, the bottom and top 25% of the data are excluded. For both MT10 and MT50 comparison  
243 against MOORE Hendawy et al. (2023), we report the success rate metrics obtained by *reproducing*  
244 the authors results by running their open-source code.<sup>2</sup>

245  
246 

#### 4.1 GRIN SHOWS BEST IQM RESULTS METAWORLD MT10

247 In Table 1, we report the evaluation success rates for MT10 in the MetaWorld environment. The  
248 mean and standard deviation of the success rate are computed across 10 random seeds. The GRIN  
249 algorithm consistently improves upon the MoE-based MTRL algorithm, despite the performance  
250 plateauing effect in MT10 also reported in (Hendawy et al., 2023). In Table 1, we also compare  
251 selected epochs with prior algorithms, including the recent PaCo (Sun et al., 2022) and MOORE  
252 approaches (Hendawy et al., 2023). We further note the MT10 success rate of  $0.8923 \pm 0.0112$   
253 reported in the recent work (Kong et al., 2025). GRIN (ours) surpasses this result, while we note  
254 that (Kong et al., 2025) reported using only 3 random seeds <sup>3</sup>.

255  
256 

#### 4.2 GRIN SHOWS SIGNIFICANT IMPROVEMENT OVER PRIOR ART ON METAWORLD MT50

257 We evaluate GRIN on the MetaWorld MT50 benchmark (MT50) with 50 distinct tasks. Our  
258 implementation builds upon the orthogonalized mixture-of-experts (MOORE) framework proposed by  
259 Hendawy et al. (Hendawy et al., 2023), employing six experts for both actor and critic networks with  
260 global activation intake and a recurrence depth of 1, as determined optimal in our ablation studies.

261 Table 2 presents the success rates and the IQM results comparing GRIN against MOORE, the current  
262 state-of-the-art method. Our results demonstrate that GRIN achieves substantial improvements over  
263 MOORE, with notable performance gains at 50M, 100M, and 175M environment steps. These  
264 results suggest that the global gating and modulation mechanism in GRIN effectively enhances  
265 the model’s ability to handle the diverse task distribution in MT50. We note that although our  
266 reproduction results with open-source code didn’t reach the reported numbers in Hendawy et al.  
267 (2023), the statistically significant improvement are clearly shown in the results. GRIN algorithm  
268 improved IQM results by **+3.7%** at 100M env. steps, shown in Table 2. This improvement sustains  
269 even as we continue to run the algorithms to 175M env. steps, as shown in Table 3.

<sup>2</sup>We used: <https://github.com/AhmedMagdyHendawy/MOORE>.

<sup>3</sup>Appendix B5 of (Kong et al., 2025)

<sup>4</sup>The success rate data for random seeds excluding bottom 25% and top 25% are all 90%.

Algorithm	Env. st.	Ave. suc.	IQM
MTSAC (Yu+ 19)	100M	49.3±1.5%	–
SAC+FiLM (Perez+ 17)	100M	36.5±12.0%	–
CARE (Sodhani+ 21)	100M	50.8±1.0%	–
PaCo (Sun+ 22)	100M	57.3±1.3%	–
MOORE (Our repro.)	50M	51.2±2.1%	–
GRIN (Ours)	50M	<b>55.7±2.9%</b>	–
MOORE (Our repro.)	100M	<b>55.7±2.8%</b>	<b>56.1±0.9%</b>
GRIN (Ours)	100M	<b>59.9±1.6%</b>	<b>59.8±0.2%</b>

Table 3: Extended run on MT50.

Table 2: Metaworld MT50 results.

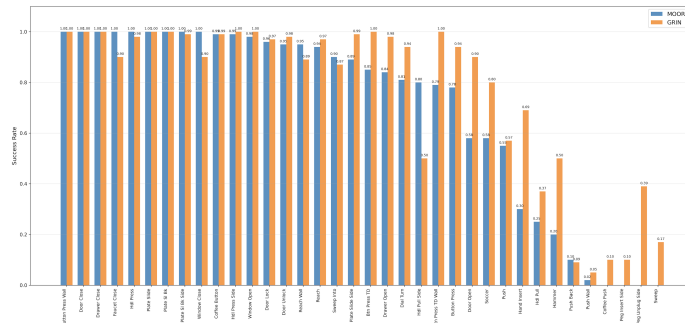


Figure 3: MT50 tasks success rate comparison GRIN compared with MOORE, reported at 50M env. steps.<sup>5</sup>

In Figure 3, we show the per-task performance of GRIN compared with the prior MOORE algorithm. Several tasks exhibit significant improvements. Out of 36 tasks with non-zero success rates, GRIN achieves higher success rates than MOORE on 22 tasks (61%). In contrast, MOORE outperforms GRIN on 8 tasks (17%).

## 4.3 ANALYSIS WITH OFF POLICY EVALUATION

In the MetaWorld MT10 environment, we perform off-policy evaluation by collecting 150,000 transitions in offline trajectories across tasks.

For each transition, Q values for GRIN, and MOORE as baseline, are computed with  $Q = F_{\text{critic}}(s_t, a_t^*)$  where  $s_t$  is the transition state, and  $a_t^* = F_{\text{actor}}(s_t)$ . During the forward compute, we collected the output representation (OR) inhibition masks, the mixture weight (MW) inhibition masks, which are used to compute average inhibition levels. Table 4 shows OR inhibition levels correlates the most with the Q value. In comparison the inhibition levels on mixture weights are less significant. This finding indicates GRIN’s modulation may play a larger role compared to routing data in MTRL. Across data in all transitions, we fit Gaussian distributions to the baseline model’s and GRIN’s Q values for a Fitted Q Evaluation (FQE) analysis. Figure 4 shows the Q value improvement with GRIN is on average 8.5, and 93.5% of the samples observed improvement in Q with GRIN. Finally, we present a segment analysis. The data is segmented by the median in actor inhibition level<sup>6</sup>. On the top of Figure 5 we show histogram plot of Q values of transitions with more actor OR inhibition (above median), and on the bottom we show the plot for transitions with less. With more inhibition, we observe more improvement (+10.2) across the median of GRIN Q values vs baseline. This value is smaller (+9.5) in the opposing segment. The value distributions are visibly different across more vs less inhibition. The result shows the effectiveness and significance of modulation from the GRIN head model.

#### 4.4 ABLATION STUDIES

<sup>6</sup>We compute the average across the hidden units for Actor OR inhibition masks, and find the median across the transitions. The median value is 0.105.

Table 4: Inh. corr. &amp; Q improvements

Metric	Value	Desc.
OR Inhibition	Corr.	
Actor $\rightarrow$ GRIN Q	+0.47	+ve
Actor $\rightarrow$ Q impr.	+0.31	+ve
Critic $\rightarrow$ GRIN Q	+0.19	Weak +ve
Critic $\rightarrow$ Q impr.	+0.14	Weak +ve
IMW Inhibition	Corr.	
Actor $\rightarrow$ Q	-0.08	Slight -ve
Critic $\rightarrow$ Q	-	Negligible
Q-Value Performance		
Improved samples	93.5%	
Mean impr.	$8.5 \pm 7.0$	
Gaussian Fits: Baseline vs GRIN		

Figure 4: FQE Gaussian fit of GRIN Q values vs Baseline.

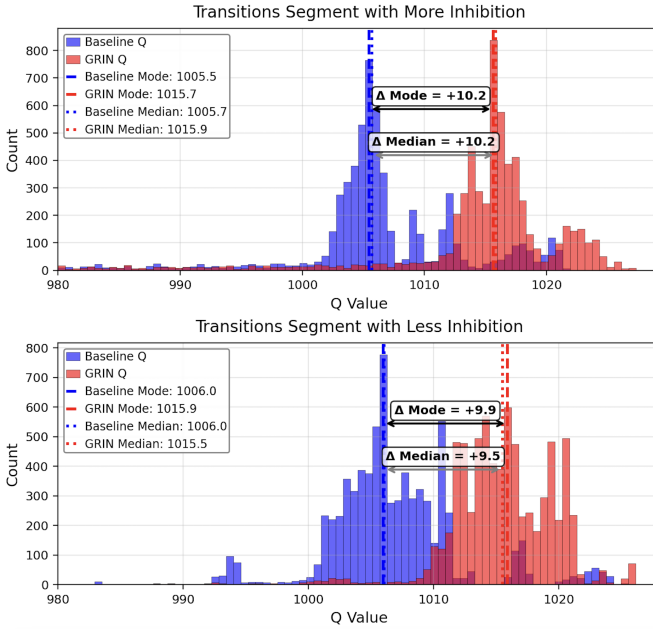


Figure 5: Segment Analysis for transitions with More OR inhibition (inhibition mask mean level is below the data median 0.105) vs Less.

**Recurrent depth.** We conduct ablation studies on the Meta-World MT5 benchmark comprising five tasks to evaluate GRIN with recurrence depths ranging from 1 to 3. The recurrent implementation follows Algorithm 1. As shown in Table 5 and Figure 6, a recurrence depth of 1 yields optimal success rates indicating a single recurrence step is typically sufficient for less complex MTRL tasks. **Number of experts.** We evaluate GRIN’s effectiveness by varying expert capacities across 3, 4, and 6 experts, keeping other parameters constant. Results in Figure 6 show that for the MT5 task, expanding the expert pool didn’t significantly improve the results. We also perform the experiment on Minigrid Chevalier-Boisvert et al. (2023) MT7<sup>7</sup> shown in Table 6 and observe similar results. Although increasing the number of experts offered less improvements, the ablation aligns with results with the MT10 Q-value correlation in Table 4, and verifies that GRIN contributes more through modulation on the representations.

**Selectivity from global inputs.** Global activations make the inhibition head effective for modulation the network. While model architectures, the selection of inputs may be needed. We offer an ablation using Minigrid, which uses a convolutional net. In the base GRIN setting, we connect the 2-D structured pretext layers to the inhibition head, while in GRIN light, we only connect the post model and the MoE output to the inhibition head. Interestingly, the light version performs well. So it may be effective to perform input selection from a global set of network activations.

**Gating mask location  $\mathcal{L}$ .** We investigate the optimal point of intervention for GRIN’s inhibition signal by applying the gating mask at three distinct locations in the MoE architecture: (a) the mixture weights that determine expert contributions ( $l^{\text{IMW}}$ ), and (b) the combined output representation after expert aggre-

Setting	Succ. rate (%)
Number of Recursion Steps	
1 step (baseline)	$91.3 \pm 8.4$
2 steps	$76.7 \pm 2.5$
3 steps	$78.0 \pm 2.8$
Number of Experts	
3 Experts (baseline)	$91.3 \pm 8.4$
4 Experts	$78.7 \pm 0.9$
6 Experts	$82.0 \pm 4.3$
Modulation and Gating Location	
OR + IMW (baseline)	$91.3 \pm 8.4$
OR only	$90.7 \pm 7.7$
MW only	$80.7 \pm 5.2$

Table 5: MT5 Ablation with GRIN

	Algorithm	4 Experts	6 Experts	8 Experts
MOORE		$74.4 \pm 7.1$	$71.5 \pm 9.3$	$78.1 \pm 3.9$
GRIN		$73.1 \pm 5.2$	$78.3 \pm 6.5$	$73.4 \pm 8.3$
GRIN light		$76.3 \pm 5.4$	$76.7 \pm 7.6$	$76.6 \pm 5.4$

Table 6: Minigrid MT7 succ. rate (%)

<sup>7</sup>Experiments were run with 10 random seeds across 50 epochs.

378 gation ( $l^{\text{OR}}$ ). We observe the inhibition mechanism is most effective at the output representation  
 379 ( $l^{\text{OR}}$ ) by selectively suppressing patterns in the aggregated output. The result aligns with the corre-  
 380 lations in Table 4, and is helpful to inform optimal architectural integration of recurrent inhibition  
 381 mechanisms.

## 383 5 GENERALIZING TO ML DOMAINS

384 The primary application of GRIN on MTRL shows its capability for state-space models. We make  
 385 efforts to generalize GRIN to other ML domains. To ensure it is efficient to grow GRIN’s parameter  
 386 size, we explore a cascade of progressively increasing input diversity.

### 388 5.1 CASCADING INPUT DIVERSITY

389 Inhibitory neurons constitute a small portion of the neural population (Swanson & Maffei, 2019),  
 390 and they exhibit remarkable diversity (Hofer et al., 2011; Pfeffer et al., 2013; Kajiwara et al., 2021).  
 391 We focus on the diversity of input connections to translate this connection diversity to the GRIN  
 392 head module ( $\mathcal{G}$ ):

393 **Pretext Inhibition (PRE):** The gating mechanism operates on incomplete forward-pass informa-  
 394 tion, using the activations available up to the current layer (the pretext). Gated Linear Unit (GLU) is  
 395 a special instance.

396 **Cross-iteration Global Inhibition (CIGI):** We processes all activations from the previous stochas-  
 397 tic optimization batch through a dedicated inhibition head to generate gating masks. Pooling opera-  
 398 tions are applied across the batch, producing sample-agnostic inhibition masks to gate the activations  
 399 of the current iteration.

400 **Global Recurrent Inhibition Network (GRIN):** GRIN algorithm was described in Section 3 which  
 401 not only can produce specific masks per data sample, but also refine the adaptive gating decisions  
 402 iteratively.

403 The inhibition head model combines information from multiple sources to compute the inhibition  
 404 masks:

$$405 \mathbf{s}_{t+1} = \sigma(\mathcal{G}(\mathbf{a}_{\text{global}})) = \sigma(\mathbb{I}_{\text{PRE}} W_{\text{PRE}} \cdot f_{\text{PRE}}(\mathbf{a}_t) + \mathbb{I}_{\text{CIGI}} W_{\text{CIGI}} \cdot f_{\text{CIGI}}(\mathbf{a}_{t-1}^*) + \mathbb{I}_{\text{GRIN}} W_{\text{GRIN}} \cdot \mathbf{h}_t + b) \quad (3)$$

406 where  $\mathbb{I}$  are indicator functions to select the existence of  
 407 the connection;  $\mathbf{a}_{t-1}^*$  represents pooled activations from  
 408 the previous batch in CIGI. At training time for CIGI,  
 409 the inhibition head and base model are jointly optimized.  
 410 At inference time, when evaluating a new data point, we  
 411 sample a batch of test data to simulate its prior iteration,  
 412 producing the pooled inhibition masks.

### 413 5.2 HAND-WRITTEN 414 DIGITS AND NUMBER OF SQUARES

415 To generalize to the vision domain, we built a bi-modal  
 416 simulated dataset comprising 120,000 samples, com-  
 417 posed of half MNIST handwritten digits and half syn-  
 418 synthetic number patterns (Stoianov & Zorzi, 2012). Each  
 419 sample is labeled with its numeric value (0-9). We use a convnet with a sparsely gated MoE with  
 420 fully connected layers (Shazeer et al., 2017).

421 Results in Table 7 show that MoE models benefit from global  
 422 inhibition gating. While dropout improves performance, it re-  
 423 quires careful hyperparameter tuning. In contrast, adaptive in-  
 424 hibition methods automatically determine appropriate signal  
 425 suppression levels, with performance scaling with connection  
 426 diversity.

### 427 5.3 LANGUAGE MODEL EXPERIMENT

428 We experiment with the transformer language model Vaswani  
 429 et al. (2017); Shazeer et al. (2017); Du et al. (2022) with GRIN.

Algorithm	Acc.	Std.
Baseline model	81.4%	1.7e-2
MoE 3/5 experts	92.3%	5.6e-2
Random (dropout 0.25)	94.9%	2.0e-2
Random (dropout 0.5)	95.1%	1.9e-2
Random (dropout 0.75)	95.9%	8.1e-3
One-layer I. (GLU)	95.2%	5.1e-3
PRE	95.3%	8.4e-3
CIGI	94.9%	2.3e-3
GRIN	<b>96.3%</b>	1.0e-2

Table 7: Results on mixed-numbers dataset

Algorithm	300K data	1M data
Baseline model	3.69e-6	1.17e-8
MoE 3/10 experts	3.68e-6	2.52e-10
PRE	3.37e-6	1.82e-10
CIGI/GRIN	<b>3.31e-6</b>	<b>1.81e-10</b>

Table 8: WMT English monolingual dataset (normalized log-likelihood loss)

432 The MoE is applied on the fully connected layers of the trans-  
 433 former model, and gating heads is applied on the input of the MoE. The LM task is applied on WMT  
 434 English monolingual dataset (Maillard et al., 2024) with one smaller set containing 300K sentences  
 435 (7.5M words) and a larger one with 1 million sentences (25M words). Following the pre-processing,  
 436 we train transformers. Table 8 shows test set normalized log-likelihood on next word prediction.  
 437 The baseline MoE without gating performs similar to standard models, indicating less optimized  
 438 routing and gating. Global inhibition yields visible improvements across both datasets, confirming  
 439 its effectiveness for LM’s.

## 440 6 CONCLUSION

442 We introduced the Global Recurrent Inhibition Network (GRIN), a novel architecture that enhances  
 443 dynamic routing in Mixture of Experts models. GRIN implements a global inhibition head that  
 444 recurrently processes diverse network activations and generate targeted gating signals. Our eval-  
 445 uation demonstrates improvements across tasks, particularly MTRL. For future work, we study the  
 446 input spaces to GRIN with architecture specific designs and apply GRIN to more domains and in the  
 447 multi-modal space. These directions enable learned optimization of gating strategies that surpass  
 448 our current architectural design.

## 449 REFERENCES

450 Rishabh Agarwal, Max Schwarzer, Pablo Samuel Castro, Aaron C Courville, and Marc Bellemare.  
 451 Deep reinforcement learning at the edge of the statistical precipice. *Advances in neural informa-*  
 452 *tion processing systems*, 34:29304–29320, 2021.

453 Jimmy Ba and Brendan Frey. Adaptive dropout for training deep neural networks. In C.J. Burges, L. Bottou, M. Welling, Z. Ghahramani, and K.Q. Weinberger (eds.), *Ad-*  
 454 *vances in Neural Information Processing Systems*, volume 26. Curran Associates, Inc., 2013. URL [https://proceedings.neurips.cc/paper\\_files/paper/2013/file/7b5b23f4aadf9513306bcd59afb6e4c9-Paper.pdf](https://proceedings.neurips.cc/paper_files/paper/2013/file/7b5b23f4aadf9513306bcd59afb6e4c9-Paper.pdf).

455 Maxime Chevalier-Boisvert, Bolun Dai, Mark Towers, Rodrigo Perez-Vicente, Lucas Willems,  
 456 Salem Lahliou, Suman Pal, Pablo Samuel Castro, and Jordan Terry. Minigrid & miniworld: Mod-  
 457 uular & customizable reinforcement learning environments for goal-oriented tasks. *Advances in*  
 458 *Neural Information Processing Systems*, 36:73383–73394, 2023.

459 Marta Chini, Thomas Pfeffer, and Ileana Hanganu-Opitz. An increase of inhibition drives the de-  
 460 velopmental decorrelation of neural activity. *eLife*, 11:e78811, 2022. doi: 10.7554/eLife.78811.  
 461 URL <https://doi.org/10.7554/eLife.78811>.

462 Yann N Dauphin, Angela Fan, Michael Auli, and David Grangier. Language modeling with gated  
 463 convolutional networks. In *International conference on machine learning*, pp. 933–941. PMLR,  
 464 2017a.

465 Yann N. Dauphin, Angela Fan, Michael Auli, and David Grangier. Language modeling with gated  
 466 convolutional networks, 2017b. URL <https://arxiv.org/abs/1612.08083>.

467 Carlo D’Eramo, Davide Tateo, Andrea Bonarini, Marcello Restelli, and Jan Peters. Sharing knowl-  
 468 edge in multi-task deep reinforcement learning. *arXiv preprint arXiv:2401.09561*, 2024.

469 Coline Devin, Abhishek Gupta, Trevor Darrell, Pieter Abbeel, and Sergey Levine. Learning mod-  
 470 uular neural network policies for multi-task and multi-robot transfer. In *2017 IEEE international*  
 471 *conference on robotics and automation (ICRA)*, pp. 2169–2176. IEEE, 2017.

472 Nan Du, Yanping Huang, Andrew M Dai, Simon Tong, Dmitry Lepikhin, Yuanzhong Xu, Maxim  
 473 Krikun, Yanqi Zhou, Adams Wei Yu, Orhan Firat, et al. Glam: Efficient scaling of language  
 474 models with mixture-of-experts. In *International conference on machine learning*, pp. 5547–  
 475 5569. PMLR, 2022.

476 Golnaz Ghiasi, Tsung-Yi Lin, and Quoc V. Le. Dropblock: A regularization method for convolu-  
 477 tional networks, 2018. URL <https://arxiv.org/abs/1810.12890>.

486 Albert Gidon and Idan Segev. Principles governing the operation of synaptic inhibition in dendrites.  
 487 *Neuron*, 75(2):330–341, 2012.  
 488

489 Shixiang Gu, Ethan Holly, Timothy Lillicrap, and Sergey Levine. Deep reinforcement learning for  
 490 robotic manipulation with asynchronous off-policy updates. In *2017 IEEE international conference on robotics and automation (ICRA)*, pp. 3389–3396. IEEE, 2017.  
 491

492 David Ha, Andrew Dai, and Quoc V Le. Hypernetworks. *arXiv preprint arXiv:1609.09106*, 2016.  
 493

494 Tuomas Haarnoja, Aurick Zhou, Pieter Abbeel, and Sergey Levine. Soft actor-critic: Off-policy  
 495 maximum entropy deep reinforcement learning with a stochastic actor. In *International conference on machine learning*, pp. 1861–1870. Pmlr, 2018.  
 496

497 Tao Han, Huaixuan Shi, Xinyi Ding, Xi-Ao Ma, Huamao Gu, and Yili Fang. Mixture of experts  
 498 based multi-task supervise learning from crowds. In *Proceedings of the AAAI Conference on Artificial Intelligence*, volume 39, pp. 14256–14264, 2025.  
 499

500 Ahmed Hendawy, Jan Peters, and Carlo D’Eramo. Multi-task reinforcement learning with mixture  
 501 of orthogonal experts. *arXiv preprint arXiv:2311.11385*, 2023.  
 502

503 Geoffrey E Hinton, Alex Krizhevsky, and Sida D Wang. Transforming auto-encoders. In *International conference on artificial neural networks*, pp. 44–51. Springer, 2011.  
 504

505 Geoffrey E Hinton, Sara Sabour, and Nicholas Frosst. Matrix capsules with em routing. In *International conference on learning representations*, 2018.  
 506

507 Sepp Hochreiter and Jürgen Schmidhuber. Long short-term memory. *Neural computation*, 9(8):  
 508 1735–1780, 1997.  
 509

510 Sonja B Hofer, Ho Ko, Bruno Pichler, Joshua Vogelstein, Hana Ros, Hongkui Zeng, Ed Lein,  
 511 Nicholas A Lesica, and Thomas D Mrsic-Flogel. Differential connectivity and response dynamics of excitatory and inhibitory neurons in visual cortex. *Nature neuroscience*, 14(8):1045–1052,  
 512 2011.  
 513

514 Jeffry S. Isaacson and Massimo Scanbiani. How inhibition shapes cortical activity. *Neuron*, 72(2):231–243, 2011. ISSN 0896-6273. doi: <https://doi.org/10.1016/j.neuron.2011.09.027>. URL <https://www.sciencedirect.com/science/article/pii/S0896627311008798>.  
 515

516 Motoki Kajiwara, Ritsuki Nomura, Felix Goetze, Masanori Kawabata, Yoshikazu Isomura, Tatsuya  
 517 Akutsu, and Masanori Shimono. Inhibitory neurons exhibit high controlling ability in the cortical  
 518 microconnectome. *PLOS Computational Biology*, 17(4):e1008846, 2021.  
 519

520 Dmitry Kalashnikov, Alex Irpan, Peter Pastor, Julian Ibarz, Alexander Herzog, Eric Jang, Deirdre  
 521 Quillen, Ethan Holly, Mrinal Kalakrishnan, Vincent Vanhoucke, et al. Scalable deep reinforcement learning for vision-based robotic manipulation. In *Conference on robot learning*, pp. 651–  
 522 673. PMLR, 2018.  
 523

524 Diederik P. Kingma, Tim Salimans, and Max Welling. Variational dropout and the local reparameterization trick, 2015. URL <https://arxiv.org/abs/1506.02557>.  
 525

526 Thomas Klausberger and Peter Somogyi. Neuronal diversity and temporal dynamics: the unity of  
 527 hippocampal circuit operations. *Science*, 321(5885):53–57, 2008.  
 528

529 Yilun Kong, Guozheng Ma, Qi Zhao, Haoyu Wang, Li Shen, Xueqian Wang, and Dacheng Tao.  
 530 Mastering massive multi-task reinforcement learning via mixture-of-expert decision transformer.  
 531 *arXiv preprint arXiv:2505.24378*, 2025.  
 532

533 Adam Kosiorek, Sara Sabour, Yee Whye Teh, and Geoffrey E Hinton. Stacked capsule autoencoders.  
 534 *Advances in neural information processing systems*, 32, 2019.  
 535

536 Bonan Li, Yinhua Hu, Xuecheng Nie, Congying Han, Xiangjian Jiang, Tiande Guo, and Luoqi Liu.  
 537 Dropkey, 2023. URL <https://arxiv.org/abs/2208.02646>.  
 538

540 Timothy P Lillicrap, Jonathan J Hunt, Alexander Pritzel, Nicolas Heess, Tom Erez, Yuval Tassa,  
 541 David Silver, and Daan Wierstra. Continuous control with deep reinforcement learning. *arXiv*  
 542 *preprint arXiv:1509.02971*, 2015.

543 Yue Liu, Christos Matsoukas, Fredrik Strand, Hossein Azizpour, and Kevin Smith. Patchdropout:  
 544 Economizing vision transformers using patch dropout, 2022. URL <https://arxiv.org/abs/2208.07220>.

545 Jiaqi Ma, Zhe Zhao, Xinyang Yi, Jilin Chen, Lichan Hong, and Ed H Chi. Modeling task relation-  
 546 ships in multi-task learning with multi-gate mixture-of-experts. In *Proceedings of the 24th ACM*  
 547 *SIGKDD international conference on knowledge discovery & data mining*, pp. 1930–1939, 2018.

548 Jean Maillard, Laurie Burchell, Antonios Anastasopoulos, Christian Federmann, Philipp Koehn,  
 549 and Skyler Wang. Findings of the WMT 2024 shared task of the open language data initiative.  
 550 In Barry Haddow, Tom Kocmi, Philipp Koehn, and Christof Monz (eds.), *Proceedings of the*  
 551 *Ninth Conference on Machine Translation*, pp. 110–117, Miami, Florida, USA, November 2024.  
 552 Association for Computational Linguistics. doi: 10.18653/v1/2024.wmt-1.4. URL <https://aclanthology.org/2024.wmt-1.4/>.

553 Henry Markram, Maria Toledo-Rodriguez, Yun Wang, Anirudh Gupta, Gilad Silberberg, and Caizhi  
 554 Wu. Interneurons of the neocortical inhibitory system. *Nature reviews neuroscience*, 5(10):793–  
 555 807, 2004.

556 Volodymyr Mnih, Koray Kavukcuoglu, David Silver, Alex Graves, Ioannis Antonoglou, Daan Wier-  
 557 stra, and Martin Riedmiller. Playing atari with deep reinforcement learning. *arXiv preprint*  
 558 *arXiv:1312.5602*, 2013.

559 Ethan Perez, Florian Strub, Harm De Vries, Vincent Dumoulin, and Aaron Courville. Film: Visual  
 560 reasoning with a general conditioning layer. In *Proceedings of the AAAI conference on artificial*  
 561 *intelligence*, volume 32, 2018.

562 Carsten K Pfeffer, Mingshan Xue, Miao He, Z Josh Huang, and Massimo Scanziani. Inhibition of  
 563 inhibition in visual cortex: the logic of connections between molecularly distinct interneurons.  
 564 *Nature neuroscience*, 16(8):1068–1076, 2013.

565 Hieu Pham, Melody Guan, Barret Zoph, Quoc Le, and Jeff Dean. Efficient neural architecture search  
 566 via parameters sharing. In *International conference on machine learning*, pp. 4095–4104. PMLR,  
 567 2018.

568 Zihan Qiu, Zekun Wang, Bo Zheng, Zeyu Huang, Kaiyue Wen, Songlin Yang, Rui Men, Le Yu, Fei  
 569 Huang, Suozhi Huang, et al. Gated attention for large language models: Non-linearity, sparsity,  
 570 and attention-sink-free. *arXiv preprint arXiv:2505.06708*, 2025.

571 Jathushan Rajasegaran, Vinoj Jayasundara, Sandaru Jayasekara, Hirunima Jayasekara, Suranga  
 572 Seneviratne, and Ranga Rodrigo. Deepcaps: Going deeper with capsule networks. In *Proceed-  
 573 ings of the IEEE/CVF conference on computer vision and pattern recognition*, pp. 10725–10733,  
 574 2019.

575 Sara Sabour, Nicholas Frosst, and Geoffrey E Hinton. Dynamic routing between capsules. *Advances*  
 576 *in neural information processing systems*, 30, 2017.

577 Noam Shazeer. Glu variants improve transformer, 2020. URL <https://arxiv.org/abs/2002.05202>.

578 Noam Shazeer, Azalia Mirhoseini, Krzysztof Maziarz, Andy Davis, Quoc Le, Geoffrey Hinton,  
 579 and Jeff Dean. Outrageously large neural networks: The sparsely-gated mixture-of-experts layer,  
 580 2017. URL <https://arxiv.org/abs/1701.06538>.

581 Shagun Sodhani, Amy Zhang, and Joelle Pineau. Multi-task reinforcement learning with context-  
 582 based representations. In *International conference on machine learning*, pp. 9767–9779. PMLR,  
 583 2021.

584 Rupesh Kumar Srivastava, Klaus Greff, and Jürgen Schmidhuber. Highway networks. *CoRR*,  
 585 abs/1505.00387, 2015. URL <http://arxiv.org/abs/1505.00387>.

594 Kenneth O Stanley, David B D’Ambrosio, and Jason Gauci. A hypercube-based encoding for evolv-  
 595 ing large-scale neural networks. *Artificial life*, 15(2):185–212, 2009.  
 596

597 Ivilin Stoianov and Marco Zorzi. Emergence of a ‘visual number sense’ in hierarchical generative  
 598 models. *Nature neuroscience*, 15(2):194–196, 2012.  
 599

600 Lingfeng Sun, Haichao Zhang, Wei Xu, and Masayoshi Tomizuka. Paco: Parameter-compositional  
 601 multi-task reinforcement learning. *Advances in Neural Information Processing Systems*, 35:  
 602 21495–21507, 2022.  
 603

604 Olivia K Swanson and Arianna Maffei. From hiring to firing: activation of inhibitory neurons and  
 605 their recruitment in behavior. *Frontiers in molecular neuroscience*, 12:168, 2019.  
 606

607 Yee Teh, Victor Bapst, Wojciech M Czarnecki, John Quan, James Kirkpatrick, Raia Hadsell, Nicolas  
 608 Heess, and Razvan Pascanu. Distral: Robust multitask reinforcement learning. *Advances in neural  
 609 information processing systems*, 30, 2017.  
 610

611 Rémi Tremblay, Sophia Lee, and Bernardo Rudy. Gabaergic interneurons in the neocortex: from  
 612 cellular properties to circuits. *Neuron*, 91(2):260–292, 2016.  
 613

614 Ashish Vaswani, Noam Shazeer, Niki Parmar, Jakob Uszkoreit, Llion Jones, Aidan N Gomez,  
 615 Łukasz Kaiser, and Illia Polosukhin. Attention is all you need. *Advances in neural informa-  
 616 tion processing systems*, 30, 2017.  
 617

618 Dilin Wang and Qiang Liu. An optimization view on dynamic routing between capsules. 2018.  
 619

620 Ruihan Yang, Huazhe Xu, Yi Wu, and Xiaolong Wang. Multi-task reinforcement learning with soft  
 621 modularization. *Advances in Neural Information Processing Systems*, 33:4767–4777, 2020.  
 622

623 Tianhe Yu, Saurabh Kumar, Abhishek Gupta, Sergey Levine, Karol Hausman, and Chelsea Finn.  
 624 Gradient surgery for multi-task learning. *Advances in neural information processing systems*, 33:  
 625 5824–5836, 2020a.  
 626

627 Tianhe Yu, Deirdre Quillen, Zhanpeng He, Ryan Julian, Karol Hausman, Chelsea Finn, and Sergey  
 628 Levine. Meta-world: A benchmark and evaluation for multi-task and meta reinforcement learning.  
 629 In *Conference on robot learning*, pp. 1094–1100. PMLR, 2020b.  
 630

631 Yiren Zhao, Oluwatomisin Dada, Xitong Gao, and Robert D Mullins. Revisiting structured dropout,  
 632 2022. URL <https://arxiv.org/abs/2210.02570>.  
 633

634 Barret Zoph and Quoc V Le. Neural architecture search with reinforcement learning. In *Inter-  
 635 national Conference on Learning Representations*, 2017.  
 636

637 Barret Zoph, Vijay Vasudevan, Jonathon Shlens, and Quoc V Le. Learning transferable architectures  
 638 for scalable image recognition. In *Proceedings of the IEEE conference on computer vision and  
 639 pattern recognition*, pp. 8697–8710, 2018.  
 640

641

642

643

644

645

646

647

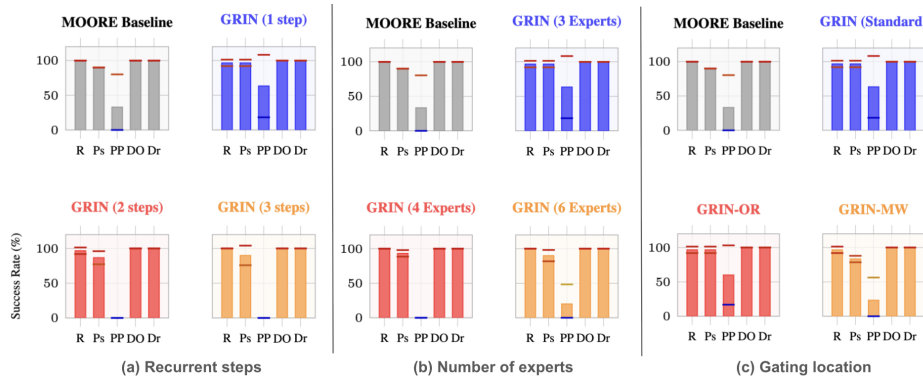


Figure 6: Ablation on MetaWorld MT5(a) Recurrent steps (b) Number of experts (c) Gating location. Task success rates (%)  $\pm$  std bars for tasks R: Reach, Ps: Push, PP: Pick Place, DO: Door Open, Dr: Drawer

## A APPENDIX

### A.1 EXTENDED BACKGROUND AND LITERATURE REVIEW

Extensions to dropout and dynamic architectures include adapting parameters through additional network models in Hypernetworks (Ha et al., 2016) and HyperNEAT (Stanley et al., 2009). Neural architecture search uses reinforcement learning to choose network architectures (Pham et al., 2018; Zoph & Le, 2017; Zoph et al., 2018).

Related to Capsules, (Wang & Liu, 2018) offers an optimization perspective, (Kosiorek et al., 2019) proposes autoencoders with capsules, and (Rajasegaran et al., 2019) builds a deeper network.

Related to MTRL, multi-task learning exists in other domains such as supervised learning (Han et al., 2025) and recommender systems (Ma et al., 2018).

### A.2 MTRL GRIN IMPLEMENTATION DETAILS

We implement GRIN in pytorch using two system generalizations. First, we leverage the forward hook registered in pytorch *nn.Module* that triggers automated storing of any activations  $a$  and their gradient computation graph. This enables the storage of activations in efficient hash data-structures. Second the pytorch module traversal is used to search global and diverse sets of inputs for the inhibition head. For efficiency, we cache the activations before  $l$  for the recurrent iterations, where  $l$  is the earliest point of dynamic modulation and gating. The caching can be done for cases where inputs are non-sequential and identical.

### A.3 ABLATION BAR CHARTS ON METAWORLD MT5 (FIGURE. 7)

### A.4 MIXED-NUMBERS AND LANGUAGE MODEL DATA AND IMPLEMENTATION DETAILS

The data set is composed of 60,000 MNIST handwritten digits and 60,000 synthetic square number patterns following (Stoianov & Zorzi, 2012). The baseline architecture employs a two-layer convolutional network with max-pooling, augmented with a sparsely gated Mixture-of-Experts layer containing 5 experts (128-unit MLPs each). K=3 experts are selected per sample via a learned router. Results in Table 7 show that MoE models benefit from global inhibition gating for handling multi-modal inputs, models with more global inhibitory connections outperform those with local inhibition on this recognition task on multi-modal vision data.

Pre-processing details for the WMT dataset: we perform lower-casing, Porter stemming, digit replacement, contraction expansion, and punctuation removal. Transformer architecture: two-layers, embedding, hidden dimension is 50, 2 heads. We use vocabulary sizes of 8,500 and 15,000 for the

702  
703  
704  
705  
706  
707  
708  
709  
710  
711  
712  
713  
714  
715  
716  
717  
718  
719  
720  
721  
722  
723  
724  
725  
726  
727  
728  
729  
730  
731  
732  
733  
734  
735  
736  
737  
738  
739  
740  
741  
742  
743  
744  
745  
746  
747  
748  
749  
750  
751  
752  
753  
754  
755  
respective datasets (300k, 1m) and models are trained with Adam with a learning rate of 0.001 and  
batch size of 256. For each MoE we use 10 experts and each data points assigns K=3 experts.

### A.5 EXPERIMENTS AND ABLATION ON MINIGRID

Table 9: MiniGrid MT7 Results at Epoch 46: Average Return across 10 random seeds

Algorithm	4 Experts	6 Experts	8 Experts
MOORE	$0.7501 \pm 0.0604$	<b><math>0.7746 \pm 0.0606</math></b>	<b><math>0.7831 \pm 0.0413</math></b>
GRIN	$0.7530 \pm 0.0545$	$0.7523 \pm 0.0490$	$0.7449 \pm 0.0761$
GRIN light	<b><math>0.7759 \pm 0.0612</math></b>	<b><math>0.7754 \pm 0.0535</math></b>	$0.7657 \pm 0.0543$

Table 10: MiniGrid MT7 Performance Comparison at Epoch 46

Experts	MOORE	GRIN	GRIN light
4	0.7501	0.7530	<b>0.7759</b>
6	0.7746	0.7523	<b>0.7754</b>
8	<b>0.7831</b>	0.7449	0.7657

Table 11: MiniGrid MT7 Detailed Results at Epoch 46

Experiment	Algorithm	Experts	Seeds	Average Return
GRIN with 4 experts	GRIN	4	10	$0.7530 \pm 0.0545$
GRIN with 6 experts	GRIN	6	10	$0.7523 \pm 0.0490$
GRIN with 8 experts	GRIN	8	10	$0.7449 \pm 0.0761$
GRIN light with 4 experts	GRIN_light	4	10	$0.7759 \pm 0.0612$
GRIN light with 6 experts	GRIN_light	6	10	$0.7754 \pm 0.0535$
GRIN light with 8 experts	GRIN_light	8	10	$0.7657 \pm 0.0543$
MOORE with 4 experts	MOORE	4	10	$0.7501 \pm 0.0604$
MOORE with 6 experts	MOORE	6	10	$0.7746 \pm 0.0606$
MOORE with 8 experts	MOORE	8	10	$0.7831 \pm 0.0413$
<b>MOORE Average</b>	<b>MOORE</b>	All	-	<b>0.7693</b>
<b>GRIN Average</b>	<b>GRIN</b>	All	-	<b>0.7612</b>

### A.6 DETAILED EXPERIMENT RESULTS

756  
757  
758  
759  
760

Table 12: MT50 Results Comparison at Epoch 4: MOORE Baseline (10 seeds) vs MOORE with GRIN (10 seeds)

Task	Success Rate		Mean J (reward)		Discounted Mean J	
	Baseline	GRIN	Baseline	GRIN	Baseline	GRIN
<b>Overall Average</b>	<b>0.4650 ± 0.4769</b>	<b>0.4848 ± 0.4764</b>	-	-	-	-
Assembly	0.0000 ± 0.0000	0.0000 ± 0.0000	231.23 ± 153.79	360.68 ± 185.50	109.23 ± 64.05	164.93 ± 77.42
Basketball	0.0000 ± 0.0000	0.0000 ± 0.0000	3.51 ± 0.74	5.40 ± 1.54	1.81 ± 0.36	2.69 ± 0.72
Bin Picking	0.0000 ± 0.0000	0.0000 ± 0.0000	3.88 ± 1.59	4.35 ± 1.60	1.98 ± 0.75	2.19 ± 0.74
Box Close	0.0000 ± 0.0000	0.0000 ± 0.0000	184.02 ± 21.20	195.41 ± 17.73	101.25 ± 10.36	106.43 ± 8.01
Button Press Topdown	0.8500 ± 0.3074	0.8600 ± 0.3007	794.87 ± 154.44	829.03 ± 116.02	323.64 ± 58.20	337.73 ± 42.97
Button Press Topdown Wall	0.7000 ± 0.4583	0.6600 ± 0.4363	728.81 ± 174.50	764.72 ± 122.01	298.81 ± 62.66	313.97 ± 45.32
Button Press	0.5400 ± 0.4055	0.6800 ± 0.4468	586.69 ± 267.03	666.91 ± 257.10	262.04 ± 112.79	295.88 ± 108.60
Button Press Wall	0.9500 ± 0.0671	0.8100 ± 0.3113	705.39 ± 143.22	703.72 ± 178.43	311.79 ± 59.57	308.64 ± 71.96
Coffee Button	0.9300 ± 0.1100	0.9700 ± 0.0900	856.20 ± 99.27	959.09 ± 80.96	392.75 ± 41.87	431.45 ± 35.74
Coffee Pull	0.0000 ± 0.0000	0.0000 ± 0.0000	7.30 ± 1.43	27.00 ± 51.27	3.74 ± 0.70	11.87 ± 20.81
Coffee Push	0.0000 ± 0.0000	0.1000 ± 0.3000	7.17 ± 0.98	77.27 ± 207.91	3.71 ± 0.42	29.56 ± 76.40
Dial Turn	0.7400 ± 0.1855	0.8600 ± 0.1114	802.69 ± 220.18	961.19 ± 103.92	358.42 ± 91.33	423.90 ± 47.50
Disassemble	0.0000 ± 0.0000	0.0000 ± 0.0000	59.09 ± 6.78	58.36 ± 1.64	31.18 ± 3.57	30.78 ± 0.87
Door Close	1.0000 ± 0.0000	1.0000 ± 0.0000	1029.50 ± 8.42	1025.88 ± 18.68	403.54 ± 5.19	401.60 ± 11.22
Door Lock	0.9800 ± 0.0600	0.9100 ± 0.1814	1000.94 ± 40.38	1009.83 ± 83.52	459.33 ± 22.30	467.73 ± 40.71
Door Open	0.3500 ± 0.4365	0.6700 ± 0.4428	631.00 ± 220.49	778.03 ± 189.37	272.43 ± 77.71	326.51 ± 64.03
Door Unlock	0.9800 ± 0.0600	0.9700 ± 0.0458	1163.95 ± 59.79	1180.55 ± 42.04	528.65 ± 28.07	537.89 ± 22.02
Drawer Close	1.0000 ± 0.0000	1.0000 ± 0.0000	1319.57 ± 71.68	1338.39 ± 28.96	625.54 ± 31.42	633.60 ± 12.69
Drawer Open	0.5800 ± 0.4750	0.8800 ± 0.2960	994.69 ± 192.38	1117.33 ± 112.02	467.22 ± 81.23	519.12 ± 47.54
Faucet Open	0.0000 ± 0.0000	0.0000 ± 0.0000	601.44 ± 8.63	610.43 ± 4.87	302.26 ± 4.04	306.25 ± 1.97
Faucet Close	0.8900 ± 0.2982	0.8900 ± 0.2982	1176.43 ± 189.00	1169.61 ± 204.14	537.53 ± 77.54	533.20 ± 83.86
Hammer	0.0900 ± 0.2119	0.1800 ± 0.3059	285.55 ± 211.38	507.40 ± 298.91	132.69 ± 86.29	225.14 ± 120.50
Hand Insert	0.2300 ± 0.2326	0.5300 ± 0.3926	162.31 ± 137.83	635.83 ± 367.14	64.69 ± 53.82	276.98 ± 160.43
Handle Press Side	1.0000 ± 0.0000	1.0000 ± 0.0000	1343.77 ± 12.74	1340.83 ± 5.25	634.97 ± 10.03	632.45 ± 4.03
Handle Press	1.0000 ± 0.0000	1.0000 ± 0.0000	1371.56 ± 15.18	1352.68 ± 27.42	659.50 ± 12.77	645.93 ± 17.97
Handle Pull Side	0.6000 ± 0.4899	0.4000 ± 0.4899	620.08 ± 506.85	404.53 ± 500.30	247.21 ± 203.04	167.70 ± 205.71
Handle Pull	0.3000 ± 0.4583	0.2300 ± 0.3951	660.42 ± 237.34	615.60 ± 213.67	295.31 ± 75.76	279.21 ± 70.74
Lever Pull	0.0000 ± 0.0000	0.0000 ± 0.0000	177.44 ± 6.72	174.44 ± 4.89	89.73 ± 2.79	88.60 ± 2.38
Peg Insert Side	0.0000 ± 0.0000	0.0000 ± 0.0000	4.61 ± 3.55	35.14 ± 92.28	2.24 ± 1.44	14.83 ± 38.07
Peg Unplug Side	0.0000 ± 0.0000	0.3100 ± 0.4346	5.24 ± 1.36	257.79 ± 387.04	2.77 ± 0.67	102.86 ± 153.54
Pick Place Wall	0.0000 ± 0.0000	0.0000 ± 0.0000	0.00 ± 0.00	0.00 ± 0.00	0.00 ± 0.00	0.00 ± 0.00
Pick Out Of Hole	0.0000 ± 0.0000	0.0000 ± 0.0000	2.68 ± 0.43	2.86 ± 0.22	1.38 ± 0.22	1.48 ± 0.11
Pick Place	0.0000 ± 0.0000	0.0000 ± 0.0000	2.47 ± 0.78	3.65 ± 0.86	1.28 ± 0.39	1.89 ± 0.43
Plate Slide	0.9800 ± 0.0400	0.9300 ± 0.1418	1075.83 ± 83.20	1044.71 ± 83.52	455.12 ± 38.62	445.87 ± 32.55
Plate Slide Side	0.9200 ± 0.1470	0.9100 ± 0.1814	914.24 ± 132.92	1009.38 ± 128.67	422.18 ± 53.74	457.21 ± 40.24
Plate Slide Back	0.9900 ± 0.0300	1.0000 ± 0.0000	1240.71 ± 47.59	1258.33 ± 50.87	562.90 ± 28.33	574.76 ± 22.92
Plate Slide Back Side	1.0000 ± 0.0000	0.8100 ± 0.2809	1252.73 ± 14.69	1127.90 ± 222.28	567.86 ± 9.06	510.63 ± 97.01
Push Back	0.0100 ± 0.0300	0.0100 ± 0.0300	7.88 ± 2.29	11.29 ± 6.97	3.79 ± 1.10	5.29 ± 3.00
Push	0.2450 ± 0.2307	0.1850 ± 0.2098	299.74 ± 244.55	329.69 ± 212.78	133.77 ± 108.93	150.47 ± 95.01
Push Wall	0.0100 ± 0.0300	0.0000 ± 0.0000	185.91 ± 266.21	363.38 ± 258.71	85.37 ± 116.02	168.76 ± 115.87
Reach	0.9400 ± 0.0663	0.9600 ± 0.0490	1342.59 ± 12.75	1346.45 ± 7.40	641.34 ± 7.54	642.01 ± 4.92
Reach Wall	0.9700 ± 0.0458	0.9600 ± 0.1200	1318.39 ± 14.23	1315.76 ± 30.08	622.43 ± 5.93	621.07 ± 14.27
Shelf Place	0.0000 ± 0.0000	0.0000 ± 0.0000	0.01 ± 0.03	0.06 ± 0.16	0.01 ± 0.02	0.03 ± 0.07
Soccer	0.4300 ± 0.3848	0.4600 ± 0.3262	427.37 ± 363.84	419.29 ± 252.71	180.68 ± 153.76	180.90 ± 105.18
Stick Pull	0.0000 ± 0.0000	0.0000 ± 0.0000	4.75 ± 1.59	5.31 ± 0.83	2.46 ± 0.75	2.75 ± 0.40
Sweep Into	0.5800 ± 0.4771	0.7300 ± 0.4051	785.79 ± 387.01	1001.91 ± 305.98	358.69 ± 169.19	457.60 ± 134.81
Sweep	0.0000 ± 0.0000	0.0000 ± 0.0000	168.00 ± 72.12	256.93 ± 171.44	79.93 ± 33.35	117.49 ± 68.80
Window Open	1.0000 ± 0.0000	0.9900 ± 0.0300	1016.99 ± 41.21	1022.67 ± 50.52	410.08 ± 20.59	411.92 ± 24.61
Window Close	1.0000 ± 0.0000	0.9000 ± 0.3000	1045.53 ± 79.82	929.26 ± 269.54	427.96 ± 40.67	379.61 ± 106.33

794  
795  
796  
797  
798  
799

Table 13: MT3 Results (3 Tasks) - Mean ± Std across 5 seeds

Experiment	Task	Success Rate	Mean J (Reward)	Discounted Mean J
MT3 Baseline (256hd, 2 layers)	Reach-v2	1.000 ± 0.000	1336.18 ± 16.97	631.05 ± 13.89
	Push-v2	0.100 ± 0.200	45.86 ± 60.89	26.69 ± 35.61
	Pick-Place-v2	0.000 ± 0.000	<b>2.15 ± 1.43</b>	<b>1.17 ± 0.74</b>
MT3 Pretext Inhi. (weights only, 256hd, 2 layers)	Reach-v2	<b>1.000 ± 0.000</b>	<b>1346.20 ± 14.14</b>	<b>642.27 ± 10.18</b>
	Push-v2	<b>0.100 ± 0.200</b>	<b>62.23 ± 55.93</b>	<b>29.98 ± 23.95</b>
	Pick-Place-v2	0.000 ± 0.000	1.67 ± 0.36	0.96 ± 0.19

808  
809

810  
811  
812  
813  
814Table 14: MT5 Results (5 Tasks) - Mean  $\pm$  Std across 5 seeds

Experiment	Task	Success Rate	Mean J (Reward)	Discounted Mean J
MT5 Baseline (256hd, 2 layers)	Reach-v2	1.000 $\pm$ 0.000	1350.54 $\pm$ 15.72	644.56 $\pm$ 12.72
	Push-v2	0.000 $\pm$ 0.000	33.10 $\pm$ 25.92	20.36 $\pm$ 16.97
	Pick-Place-v2	0.000 $\pm$ 0.000	1.85 $\pm$ 0.44	1.06 $\pm$ 0.28
	Door-Open-v2	0.000 $\pm$ 0.000	458.59 $\pm$ 44.02	215.29 $\pm$ 21.55
	Drawer-Open-v2	0.000 $\pm$ 0.000	<b>738.09 <math>\pm</math> 25.11</b>	<b>358.31 <math>\pm</math> 9.54</b>
MT5 Pretext Inhibition (weights + features, 256hd, 2 layers)	Reach-v2	1.000 $\pm$ 0.000	1340.13 $\pm$ 15.30	636.03 $\pm$ 11.92
	Push-v2	0.000 $\pm$ 0.000	17.82 $\pm$ 17.18	8.86 $\pm$ 7.57
	Pick-Place-v2	0.000 $\pm$ 0.000	1.46 $\pm$ 0.49	0.87 $\pm$ 0.28
	Door-Open-v2	0.000 $\pm$ 0.000	439.82 $\pm$ 120.14	203.16 $\pm$ 47.28
	Drawer-Open-v2	0.000 $\pm$ 0.000	675.73 $\pm$ 110.36	331.72 $\pm$ 48.61
MT5 Pretext Inhibition (weights only, 256hd, 2 layers)	Reach-v2	<b>1.000 <math>\pm</math> 0.000</b>	<b>1351.29 <math>\pm</math> 16.27</b>	<b>648.46 <math>\pm</math> 7.86</b>
	Push-v2	0.000 $\pm$ 0.000	10.97 $\pm$ 8.08	6.31 $\pm$ 5.08
	Pick-Place-v2	0.000 $\pm$ 0.000	1.68 $\pm$ 0.38	0.94 $\pm$ 0.33
	Door-Open-v2	0.000 $\pm$ 0.000	457.90 $\pm$ 85.74	213.64 $\pm$ 34.67
	Drawer-Open-v2	0.000 $\pm$ 0.000	716.92 $\pm$ 30.14	349.03 $\pm$ 14.12
MT5 GRIN (rec=1) (weights + features, 256hd, 2 layers)	Reach-v2	1.000 $\pm$ 0.000	1311.13 $\pm$ 50.76	624.66 $\pm$ 19.35
	Push-v2	0.000 $\pm$ 0.000	<b>43.07 <math>\pm</math> 18.62</b>	<b>21.90 <math>\pm</math> 10.27</b>
	Pick-Place-v2	0.000 $\pm$ 0.000	2.02 $\pm$ 1.07	1.18 $\pm$ 0.59
	Door-Open-v2	0.000 $\pm$ 0.000	459.95 $\pm$ 33.94	217.50 $\pm$ 12.51
	Drawer-Open-v2	0.000 $\pm$ 0.000	718.56 $\pm$ 21.37	350.56 $\pm$ 8.39
MT5 GRIN (rec=3) (weights + features, 256hd, 2 layers)	Reach-v2	0.900 $\pm$ 0.200	1306.11 $\pm$ 72.21	627.65 $\pm$ 28.29
	Push-v2	0.000 $\pm$ 0.000	36.23 $\pm$ 22.20	18.57 $\pm$ 10.37
	Pick-Place-v2	0.000 $\pm$ 0.000	<b>2.37 <math>\pm</math> 1.56</b>	<b>1.26 <math>\pm</math> 0.80</b>
	Door-Open-v2	0.000 $\pm$ 0.000	409.93 $\pm$ 91.58	195.16 $\pm$ 40.73
	Drawer-Open-v2	0.000 $\pm$ 0.000	733.90 $\pm$ 48.66	356.60 $\pm$ 23.27
MT5 GRIN (rec=1) (weights only, 256hd, 2 layers)	Reach-v2	0.900 $\pm$ 0.200	1313.09 $\pm$ 58.16	626.27 $\pm$ 24.21
	Push-v2	0.000 $\pm$ 0.000	26.70 $\pm$ 7.30	15.13 $\pm$ 3.82
	Pick-Place-v2	0.000 $\pm$ 0.000	1.95 $\pm$ 0.59	1.06 $\pm$ 0.23
	Door-Open-v2	0.000 $\pm$ 0.000	<b>461.62 <math>\pm</math> 17.06</b>	<b>217.69 <math>\pm</math> 7.55</b>
	Drawer-Open-v2	0.000 $\pm$ 0.000	722.52 $\pm$ 17.35	351.05 $\pm$ 9.82

834  
844  
845  
846  
847  
848  
849  
850  
851

Table 15: MT10 Results Comparison at Epoch 20: MOORE Baseline (9 seeds) vs MOORE with GRIN (10 seeds)

Task	Success Rate		Mean J		Discounted Mean J	
	Baseline	GRIN	Baseline	GRIN	Baseline	GRIN
<b>Overall Average</b>	<b>0.8844 <math>\pm</math> 0.3137</b>	<b>0.8820 <math>\pm</math> 0.3135</b>	-	-	-	-
Reach	0.9778 $\pm$ 0.0629	0.9700 $\pm$ 0.0900	1350.86 $\pm$ 9.58	1351.25 $\pm$ 12.89	643.48 $\pm$ 7.06	645.07 $\pm$ 9.72
Push	1.0000 $\pm$ 0.0000	0.9500 $\pm$ 0.1025	1165.10 $\pm$ 92.92	1180.19 $\pm$ 94.50	507.36 $\pm$ 61.12	526.68 $\pm$ 53.01
Pick Place	0.0000 $\pm$ 0.0000	0.0000 $\pm$ 0.0000	2.78 $\pm$ 0.84	4.83 $\pm$ 2.01	1.42 $\pm$ 0.43	2.45 $\pm$ 0.92
Door Open	1.0000 $\pm$ 0.0000	1.0000 $\pm$ 0.0000	1067.50 $\pm$ 21.55	1043.79 $\pm$ 45.21	445.38 $\pm$ 12.66	432.47 $\pm$ 21.60
Drawer Open	0.8778 $\pm$ 0.3119	1.0000 $\pm$ 0.0000	1203.17 $\pm$ 165.46	1266.55 $\pm$ 22.76	562.34 $\pm$ 71.38	587.66 $\pm$ 11.94
Drawer Close	1.0000 $\pm$ 0.0000	1.0000 $\pm$ 0.0000	1359.86 $\pm$ 4.67	1354.25 $\pm$ 4.49	647.33 $\pm$ 4.10	642.47 $\pm$ 3.87
Button Press Topdown	1.0000 $\pm$ 0.0000	1.0000 $\pm$ 0.0000	906.88 $\pm$ 14.24	880.70 $\pm$ 25.45	372.22 $\pm$ 7.41	358.76 $\pm$ 12.05
Peg Insert Side	0.9889 $\pm$ 0.0314	0.9000 $\pm$ 0.3000	1096.05 $\pm$ 30.69	1037.75 $\pm$ 144.47	453.41 $\pm$ 13.36	423.62 $\pm$ 59.19
Window Open	1.0000 $\pm$ 0.0000	1.0000 $\pm$ 0.0000	1083.37 $\pm$ 17.57	1078.88 $\pm$ 22.52	443.51 $\pm$ 11.29	446.55 $\pm$ 13.32
Window Close	1.0000 $\pm$ 0.0000	1.0000 $\pm$ 0.0000	1063.78 $\pm$ 45.47	1082.34 $\pm$ 21.52	435.26 $\pm$ 23.63	444.50 $\pm$ 13.98

862  
863